www.czasopisma.pan.pl PAN www.journals.pan.pl
Opto-Electronics Review 25 (2017) 181–187

Contents lists available at ScienceDirect

Opto-Electronics Review

journal homepage: http://www.journals.elsevier.com/opto-electronics review

Review

Carrier transport mechanisms in the ZnO based heterojunctions grown by MBE☆

E. Płaczek-Popko[a,*], K.M. Paradowska[a], M.A. Pietrzyk[b], A. Kozanecki[b]

[a] Department of Quantum Technologies, Faculty of Fundamental Problems of Technology, Wroclaw University of Science and Technology, Wybrzeze Wyspianskiego 27, 50-370 Wroclaw, Poland
[b] Institute of Physics, Polish Academy of Sciences, al. Lotnikow 32/46, PL-02-668 Warsaw, Poland

ARTICLE INFO

Article history:
Received 18 January 2017
Received in revised form 20 April 2017
Accepted 16 June 2017
Available online 12 July 2017

Keywords:
Current transport
Tunneling current
ZnO/Si heterojunction

ABSTRACT

This paper presents a review of models of the current transport in different kind of heterojunctions (HJs) and their characteristics. In order to effectively deduce the dominant electron transport for the HJs based on ZnO or $Zn_{1-x}Mg_xO$ layers grown on Si substrate by MBE a comparison is performed – which type of the HJ exhibits better electrical properties. The current–voltage characteristics for the studied HJs were measured within 280–300 K. The transport properties of the HJs are explained in terms of Anderson model with reference to aforementioned current transport models. It is found, that the mechanisms of current transport for all of the studied HJs are similar. At a low forward voltage bias the tunneling current dominates while at medium voltage bias (0.5–1 V) multitunneling capture-emission prevails with the electron trap located at 0.1–0.25 eV below the bottom of a ZnO ($Zn_{1-x}Mg_xO$) conduction band. Beyond this voltage bias space charge limited current governs the current transport.

Contents

1. Introduction

Carrier transport mechanisms in semiconductor devices based on heterojunctions (HJs) decide on their performance. Therefore, the knowledge about the dominant current contributions is of crucial importance. Depending on the structure of a HJ, applied forward bias and temperature, there are different mechanisms that dominate the observed current. Various carrier transport models have been observed by authors of published papers investigating the ZnO-Si HJs. In Ref. [1] current transport was studied in the n-ZnO grown by metal organic chemical vapour deposition technique (MOCVD) on *p*-type Si (111) substrate at 650 °C. It was shown that the tunneling mechanism via deep-level states was the main conduction process at low forward bias, while space-charge-limited current conduction dominated the carrier transport at higher bias. In Ref. [2] it was shown that the current transport in n-ZnO/p-Si heterojunction diode fabricated by the sol–gel method was governed by the tunneling and space charge limited currents with an exponential distribution of traps in the band gap. The authors of Ref. [3] argued that in the case of the ZnO/Si heterojunctions the recombi-

☆ This article is an expanded version of the scientific reports presented at the International Conference on Semiconductor Nanostructures for Optoelectronics and Biosensors 2016 ICSeNOB2016, May 22–25, 2016, Rzeszow, Poland.

* Corresponding author.
E-mail address: ewa.popko@pwr.edu.pl (E. Płaczek-Popko).

http://dx.doi.org/10.1016/j.opelre.2017.06.010
1896-3757/

nation tunneling path is provided by a highly dislocated and thin n-type region created at the interface between ZnO and Si, which is generated to relieve the strain caused by the lattice mismatch. In Ref. [4] it is reported that a multi-step tunneling mechanism dominates the *I–V* characteristics of the nanocrystalline zinc oxide (nc-ZnO) films prepared by a sol–gel process on p-type single-crystalline Si substrates. The authors of Ref. [5] found that for ZnO layers grown on Si by photoinduced electro deposition method in a low voltage region, the forward current was also dominated by the multi-step tunneling model.

Also in the case of the HJs based on ZnO nanorods, similar transport mechanisms were reported. In Ref. [6] it was concluded that the recombination-tunneling mechanism was dominating the forward *I–V* characteristics in the *n*-ZnO/*p*-Si heterojunction prepared by the hydrothermal method. In Ref. [7] the HJ of ZnO nanorods grown by chemical bath deposition technique on Si substrate was studied. It was concluded that in the low forward bias region the current is dominated by a trap assisted multi-step tunneling process.

The authors of those papers agree that trap-mediated tunneling or/and space charge limited currents dominate the current transport in the ZnO-Si HJs, no matter what is the method of the ZnO layer/nanorods growth. While hydrothermal bulk growth, vapour phase transport, chemical transport techniques and flux growth techniques are standard techniques for fabrication of bulk ZnO, metal organic vapour phase epitaxy (MOVPE), molecular beam epitaxy (MBE), pulsed laser deposition (PLD) and atomic layer deposition (ALD) are used to develop advanced structures and for research purposes [6–9].

This paper describes various models of current transport in an HJ and its characteristics to effectively deduce the dominant electronic transport for the HJs based on ZnO or $Zn_{1-x}Mg_xO$ layers grown on Si substrate by MBE method. To the best of our knowledge there is very little known about current transport in the ZnO based – Si HJs made by this method. Moreover, there are no reports on the current transport for n-$Zn_{1-x}Mg_xO$/p-Si HJs. Current–voltage (*I–V*) characteristics are measured for both types of HJs as a function of temperature and analyzed using the models of current transport and Anderson model of an HJ. It was found that the presence of traps of activation energy 0.1–0.25 eV, located in the ZnO (or $Zn_{1-x}Mg_xO$) layer of the studied HJs plays crucial role in the current transport within measured temperature range and that it is a multitunneling capture-emission current. Additionally, the aim was to examine how the replacement of the ZnO layer by the $Zn_{1-x}Mg_xO$ layer affects the rectifying properties of the HJs.

2. Current transport mechanisms

The current mechanisms in a p–n junction can be identified using the basic equation of the rectification model [10]:

$$J(V,T) = J_0(T)[\exp(A(T))V - 1]. \quad (1)$$

$J_0(T)$ is the saturation current, and it is usually thermally activated:

$$J_0 \sim \exp\left(\frac{-E_{ac}}{kT}\right), \quad (2)$$

where E_{ac} stands for the activation energy and k – Boltzmann constant. The formulae for various current transport mechanisms are collected in Table 1. In the table also the equations defining $A(T)$ and corresponding ideality factors $n = AkT/q$ are given.

The first mechanism corresponding to the ideal p–n junction refers to the diffusion current J_{diff} with the thermal activation energy equal to the band gap energy, E_g. The second one – to the recombination current at the depletion region with the activation energy equal to $E_g/2$. In the case of a single recombination level at the mid gap the ideality factor $n = 2$. If there is a continuous trap distribution, then the value of ideality factor $1 < n < 2$.

Table 1
Saturation current density J_0, parameter A and ideality n factor for different current transport mechanisms at a forward-biased p–n heterojunctions.

Current transport mechanism	J_0	A	n
Diffusion	$J_0 \sim \exp\left(\frac{-E_g}{kT}\right)$	$\frac{q}{kT}$	1
Recombination	$J_0 \sim \exp\left(\frac{-E_g}{2kT}\right)$	$\frac{q}{kT}$	2
Thermionic	$J_0 \sim \exp\left(\frac{-q\nu_B}{kT}\right) kT^{3/2}$	$\frac{q}{kT}$	1
Multistep tunneling	$J_0 \sim \exp(\gamma T)$	*const*	$n \neq const$
Recombination-tunneling	$J_0 \sim N_t$	*const*	$n \neq const$
Multitunneling capture-emission	$J_0 \sim \exp\left(\frac{-E_{ac}}{kT}\right)$	*const*	$n \neq const$

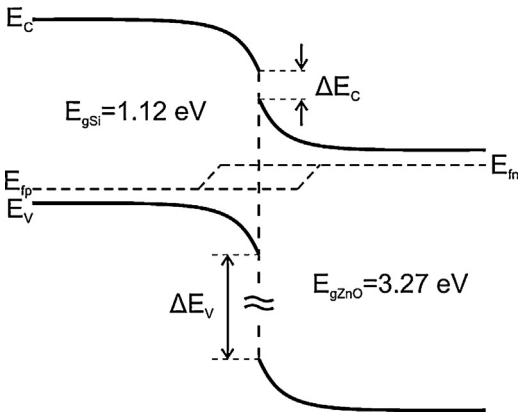

Fig. 1. Schematic energy band diagram for the forward-biased n-ZnO/p-Si heterojunction (positive bias applied to p-Si and negative bias – to n-ZnO).

For an asymmetric HJ, with one side of the junction heavily doped compared to the other side, thermionic emission governs the current transport and the HJ can be treated as a Schottky diode [10].

Before studying possible tunneling mechanisms, let us analyze the forward-biased n-ZnO/p-Si band diagram shown in Fig. 1. When n-ZnO makes an intimate contact with p-Si, the carriers diffusion current flows due to the concentration gradient. Ionized donors in ZnO form positive and ionized acceptors in Si – negative space charge near the interface. As a result the band bends upward in n-ZnO and downward in p-Si. According to the Anderson model, the conduction band offset is $\Delta E_c = \chi_{ZnO} - \chi_{Si} = 3.7 - 4.05 = -0.35$ eV [11] where χ_{ZnO} and χ_{Si} stand for electron affinity in ZnO and Si, respectively. The valence band offset is $\Delta E_V = E_{g_{ZnO}} - E_{g_{Si}} - \Delta E_c = 3.27 - 1.12 + 0.35 = 2.5$ eV. The large difference between the band offsets ΔE_c and ΔE_V results in a much lower barrier for electrons than for holes.

The possible tunneling mechanisms for a forward-biased HJ of p-Si/n-$Zn_{1-x}Mg_xO$ are shown in Fig. 2a and b. In the case of the studied here $Zn_{0.9}Mg_{0.1}O$ the conduction band offset is positive and equal to $\Delta E_C = \chi_{ZnMgO} - \chi_{Si} = 4.1 - 4.05$ eV $= 0.05$ eV, and the valence band offset is $\Delta E_V = E_{g,ZnMgO} - E_{g,Si} - \Delta E_C = 3.6 - 1.12$ eV $- 0.05$ eV $= 2.53$ eV [12]. The conduction band offset is positive, and may result in a spike, shown in both Fig. 2a and b. Like in the case of the n-ZnO/p-Si HJ there is a very low barrier for electrons and a high barrier (2.53 eV) for holes at a low forward bias. This single-carrier electron injection behaviour results in a wider depletion layer in the n-$Zn_{0.9}Mg_{0.1}O$ side, and as it will be shown below, in the space-charge limited forward current. Actually, the fact that the depletion region is mainly located in the n-side of the studied HJs has been confirmed by capacitance-voltage measurements [9].

The direct tunneling of electrons through the spike is labeled as the transition A in Fig. 2a. A single trap-mediated tunneling mech-

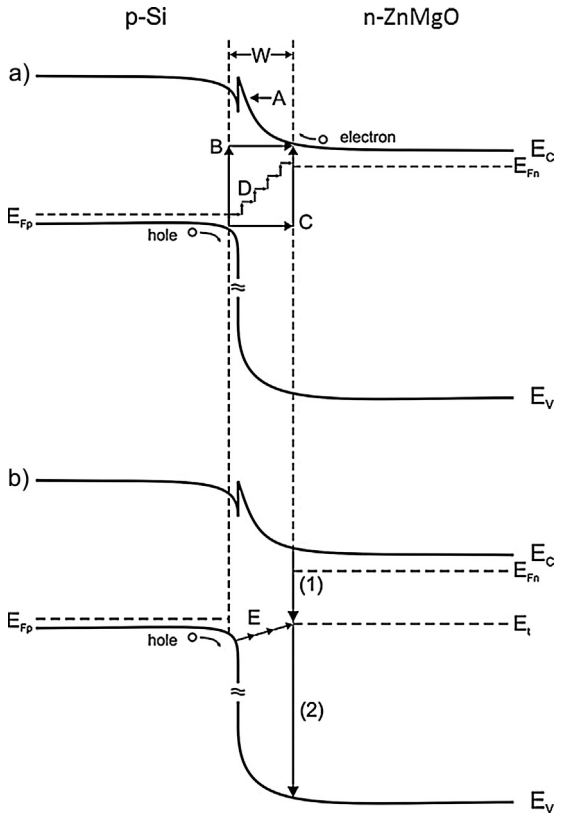

Fig. 2. Forward-biased n-$Zn_{0.9}Mg_{0.1}O$/p-Si HJ and various tunneling mechanisms (a) direct tunneling of electrons (A), single trap hole tunneling (B and C), multistep hole tunneling (D) and (b) multi-tunneling capture-emission (E): (1) – electron capture, (2) – hole emission. E_t – trap level.

anisms are labeled in Fig. 2a as the transitions B and C and the multistep tunneling as the transition D. The tunneling mechanisms B, C, D and E are presented for holes tunneling from the p-side to the n-side of the HJ because in the case of the p-Si/n-$Zn_{0.9}Mg_{0.1}O$ (or ZnO) HJ the barrier for holes is thinner than the barrier for electrons and, thus the tunneling of holes is more probable than the tunneling of electrons. Moreover, it is also assumed that the defects are located mainly in the ZnO or $Zn_{0.9}Mg_{0.1}O$ side of the interface [3]. Both materials exhibit different lattice constants which results in lattice mismatch and high concentration of defects at the n-ZnO (or $Zn_{0.9}Mg_{0.1}O$)/p-Si interface.

For the single trap tunneling mechanism the saturation current is constant, proportional to the trap concentration $J_0 \sim N_t$ and the parameter A for the hole tunneling from the p-side to n-side is expressed by the equation [13]:

$$A = \left(\frac{8\pi}{3h}\right)(m_h^*\varepsilon_1\varepsilon_0)^{1/2}N_D/[N_A^{1/2}(N_A+N_D)]. \tag{3}$$

In Eq. (3), m_h^* stands for the effective mass for holes, ε_1 is the semiconductor dielectric constant, N_D is the donor concentration, N_A is the acceptor concentration, and h is Planck's constant. It can be noted, that this equation enables calculation of N_D if N_A is known and vice-versa.

In the case of the multistep tunneling the saturation current is exponential function of temperature but the parameter $A = const$, like for the single trap tunneling. This model assumes tunneling through defects to the other side of the HJ in the interface between the two semiconductors and is shown as mechanism (D) in Fig. 2a. As it has been discussed in Ref. [13] tunneling current by one-step tunneling [B or C in Fig. 2a] is always smaller than that by multitunneling (D in the figure).

For the multitunneling capture-emission process (MTCE) [14] saturation current is a complex function, given by following equations:

$$J_0 = B[\sigma_n v_{th} N_c \exp\left(-\frac{E_c - E_T}{kT}\right) + \sigma_p v_{th} N_v \exp\left(-\frac{E_F - E_v}{kT}\right), \tag{4}$$

This equation was initially derived for n-amorphous Si/p-crystalline Si (n-aSi/-p-cSi) HJ [14]. The first term in Eq. (4) describes electron capture and the second – the hole emission, σ_n (σ_n) stands for electron (hole) capture cross section, v_{th} is the thermal velocity of carriers, $N_c(N_v)$ – density of states at the bottom of conduction band (top of valence band), $E_c - E_T$ – the distance of a trap level from the bottom of conduction band, $E_F - E_v$ – the distance of Fermi level from the top of the valence band and $B = const$. In the case of the studied here HJ it is assumed that the n-ZnO or $Zn_{0.9}Mg_{0.1}O$ layer plays similar role to the amorphous Si in the n-aSi/-p-cSi. The MTCE process is shown in Fig. 2b. Carriers tunnel through defects until they are emitted to the valence band or recombine with an electron from the conduction band, shown as mechanisms (1) and (2) in Fig. 2b, respectively.

It must be noted that different transport processes may take place at the barrier of an HJ, whereas the measured current density will usually be dominated by only one of the transport mechanisms. A summary of the several charge transport mechanisms is given in Table 1 [15].

Up to this point, it was assumed that the semiconductors were in low injection limit, i.e. $\Delta n \ll n_{n0}$ in the n-type and $\Delta p \ll p_{p0}$ in the p-type material. At high injection (sufficient applied bias and a thin enough layer) the electric field is not zero in the quasi-neutral region and the drift current becomes much larger than the diffusion current. This current is known as space charge limited currents (SCLC). It was shown, that in the absence of traps, the SCLC is a square function of applied voltage bias, V [16]:

$$J_{sclc} = \varepsilon_s \frac{\mu_n}{2L^3} V^2, \tag{5}$$

where μ_n is the carrier mobility and L is the length of the space-charge region. However in the presence of traps:

$$J_{sclc} = K \cdot V^m, \quad \text{with} \quad m > 2. \tag{6}$$

Furthermore, for exponential trap distribution m can reach pretty high value [15]:

$$m = \frac{T_T}{T} + 1, \quad \text{where} \quad N_T(E) = N_0 \exp\left(\frac{E - E_c}{kT_T}\right). \tag{7}$$

If the sample contains traps, some of the injected carriers are trapped and others remain free. As the applied voltage increases the injected carriers' charge also increases and more and more traps are filled with carriers. The voltage at which all the traps are filled is known as the trap filled limit voltage (V_{TFL}). SCLC is of great practical interest because the operating of a semiconductor device drastically changes once the V_{TFL} is achieved [17].

3. MBE technique of the ZnO/ZnMgO structures growth

The ZnO/Zn_xMg_xO structures were grown by means of the MBE technique on p-type Si (111) substrates with resistivity equal to 0.1 Ω cm. At first the Si substrates were chemically and thermally etched. Then, the substrates were placed in an ultra-high vacuum chamber and annealed at 700 °C. In the next step the growth of a thin (a few nm) Zn (or Mg) layer (to prevent Si layer from oxidation) was followed by the growth of the ZnO/Zn_xMg_xO layers at the temperature equal to 500 °C. The cross sections of the investigated HJs are shown in Fig. 3. The two samples differ in a thin MgO layer separating the $Zn_{1-x}Mg_xO$ layer from the Si substrate for the sample 1.

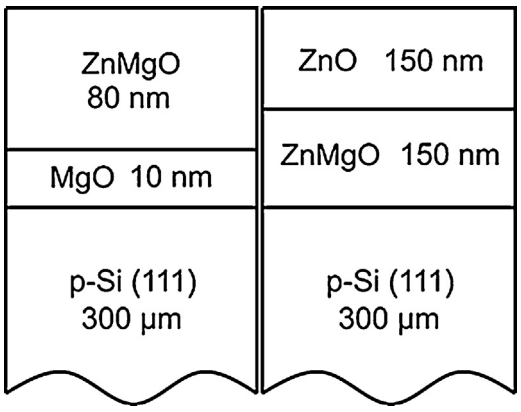

Fig. 3. The cross sections of n-$Zn_{1-x}Mg_{-x}O$/p-Si HJs.

Moreover, two other types of structures were processed. These contained $Zn_{1-x}Mg_xO$ nanocolumns grown on Si (111) substrates with a low temperature buffer ZnO layers by using MBE method. The typical structures consisted of a 350 nm thick ZnO buffer grown at low temperature (450 °C), followed by a 230 nm thick $Zn_{1-x}Mg_xO$ barrier and quantum structures grown at 800 °C. A 10 period ZnO/$Zn_{1-x}Mg_xO$ multiquantum wells (MQWs) were grown on top of these barriers. The thickness of the barrier layers was kept at about 2 and 15 nm, while that of the quantum wells ranged from 1.7 and 3 nm. The cross sections of the structures containing MQWs are shown in Fig. 4.

The crystalline quality of $Zn_{1-x}Mg_xO$/ZnO nanostructures was verified by RHEED during growth. The Mg content in $Zn_{1-x}Mg_xO$ alloy was found to be x∼10% [9].

For the electrical characterization of the HJs the ohmic contacts were deposited: Ti/Au on the top of the ZnO or $Zn_{1-x}Mg_xO$ layer and Ni/Au on the Si substrate. The *I–V* characteristics were measured within the 270–350 K range of temperature with the use of a Keithley 2601 *I–V* source-meter and a Janis cryostat with a LakeShore temperature controller.

It has to be pointed out that in the case of the samples MQW1 and MQW2 the p–n HJ is formed between p-Si substrate and n-ZnO buffer layer while for the samples 1 and 2 between the p-Si substrate and $Zn_{1-x}Mg_xO$ layer. The thin MgO layer for the sample 1 can be neglected because it is thin enough to enable tunneling. The same is true for the quantum wells, which do not affect the current transport through the p–n HJ but the contribution to the series resistance.

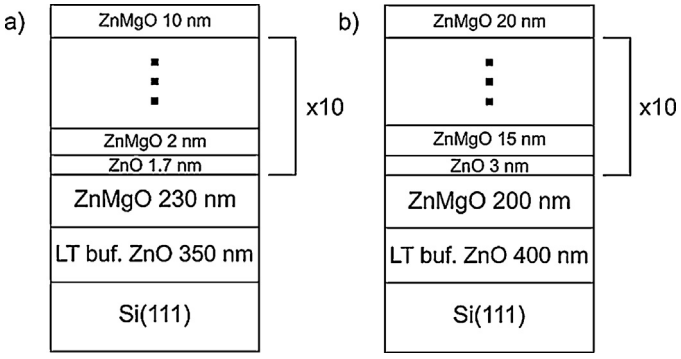

Fig. 4. The cross sections of the structures containing MQWs. (a) MQW1, (b) MQW2.

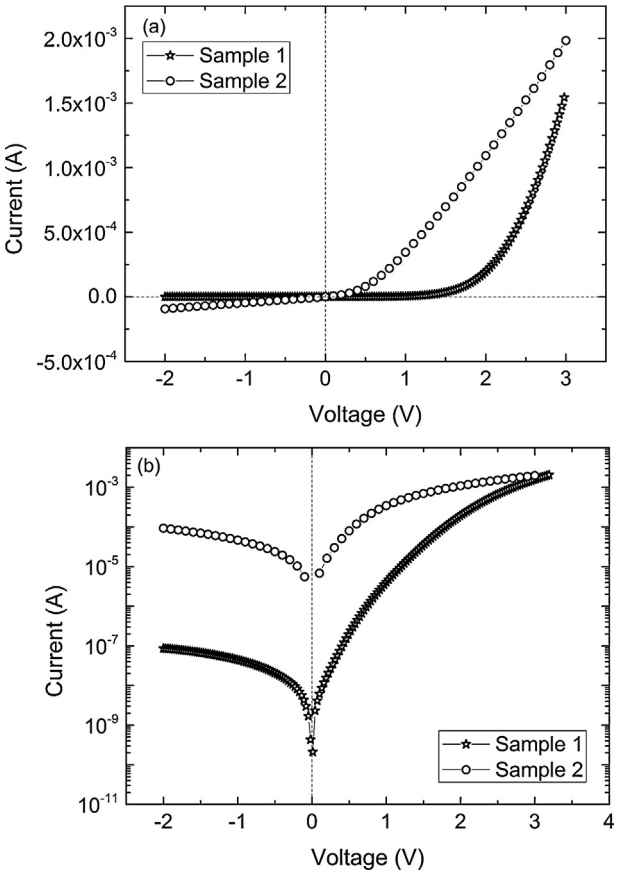

Fig. 5. Room temperature *I–V* characteristics of the samples 1 and 2 in a linear (a) and semi-logarithmic (b) scales.

4. Results and discussion

4.1. HJ n-$Zn_{0.9}Mg_{0.1}O$/p-Si

In Fig. 5. the room temperature *I–V* characteristics of the samples 1 and 2 are shown.

In Table 2 the basic junction parameters of the samples 1 and 2 obtained from the *I–V* characteristics are given. Both samples exhibit rectifying properties, but the sample 1 is much better than the other one. The rectification ratio is larger and ideality factor as well as series resistance are smaller for the sample 1. Built-in voltage for the sample 1 is equal to 2.44 eV in accordance with the Anderson model. In the case of the sample 2 it is much smaller equal only 0.7 eV, the value frequently reported for ZnO/Si HJ [18–20]. The main reason is presumably the presence of interface states which leads to the Fermi level pinning at the ZnMgO/Si interface. The presence of these states confirms higher ideality factor for the latter sample.

It was found that the saturation current for both diodes follows the relationship given by Eq. (2). The Arrhenius plots of the saturation current are shown in Fig. 6a and b. A linear fit in the high temperature range of the plots presented in Fig. 6a and b yield activation energy of about 0.25 eV and 0.16 eV, for the samples 1 and

Table 2
Room temperature rectification ratio, ideality factor, n, built-in voltage, V_{bi}, and series resistance, R_S, of the samples 1 and 2.

T (K)	Rectification ratio at ±2 V	n	V_{bi} (eV) (*I–V*)	R_S (Ω)
310	2×10^3	3.7	2.44 ± 0.07	247 ± 6
310	14	5.6	0.7 ± 0.03	907 ± 11

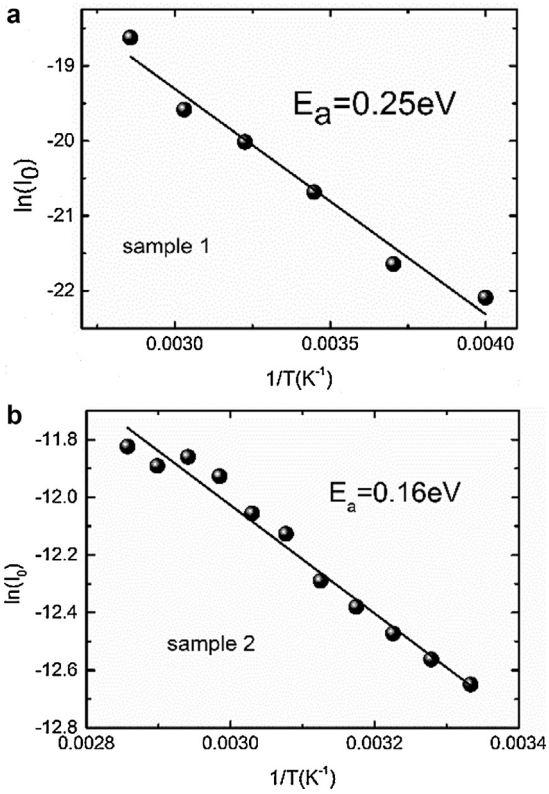

Fig. 6. The Arrhenius plot of the saturation current (a) for the sample 1 and (b) for the sample 2.

2, respectively. Both values are much smaller than the band gap energy of $Zn_{0.9}Mg_{0.1}O$. This supports the hypothesis that the diffusion and recombination current in the depletion region are not the main mechanisms causing the low forward bias current, since the activation energies for these two mechanisms are on the order of the band gap energy (much larger than those determined by us).

In Fig. 7 the *I–V* curves for both samples are shown in a double logarithmic scale (at two different temperatures). For the sample 1 three regions can be distinguished. At a low voltage bias (<0.2 V at 350 K and <0.3 V at 270 K) the slope of the plots is close to 1, indicating the Ohmic region (I). This region is missing for the sample 2, but this is presumably effect of poor resolution of the measurements for this sample. In the second region (II), at a voltage bias up

Table 3
Room temperature rectification ratio, ideality factor, n, built-in voltage, V_{bi}, and series resistance, R_S, of the samples MQW1 and MQW2.

	Rectification ratio at ±1 V	n	V_{bi} (eV) (*I–V*)	R_S (Ω)
MQW1	10	2.7	1.66	1109
MQW2	10	4.2	2.72	22

to 0.8 V for the sample 1 at 350 K and up to 1 V for the same sample at 270 K the log–log plots obey the relationship characteristic for recombination-tunneling, multisteptunneling or MTCE current. The same holds for the sample 2, however here the tunneling current dominates up to ~0.5 V. Taking into account the dependence of saturation current density on temperature (Fig. 6a and b) it may be assumed that this is the MTCE process which governs the current transport in both samples in the low forward bias.

At a larger voltage bias, space charge limited current comes to play a role. The injection current is dominated by the injected electrons under the forward voltage and the single-carrier current forms because the barrier is much higher for the holes than that for the electrons (cf. Figs. 1 and 2a, b). The slope $m > 2$ for the sample 1 indicates the SCLC with contribution of exponentially distributed traps. SCLC for the sample 2 obeys the V^2 law indicating that all the traps are already filled at 0.5 V but at a voltage >1 V the slope decreases because of the series resistance. The series resistance is decreasing with increasing temperature; therefore the influence of the resistance is more significant at 300 K than in 350 K.

Hence, the transport mechanism in the samples 1 and 2 is dominated by direct tunneling at lower voltages (region I), multitunneling capture-emission current at medium voltages (region II) and by space-charge-limited current at higher voltages (region III).

4.2. HJ n-ZnO/p-Si

The samples with MQWs differ from the samples 1 and 2 because in these samples the junction is formed between p-Si and n-ZnO instead of $Zn_{0.9}Mg_{0.1}O$. In Table 3 the basic junction parameters of the samples MQW1 and MQW2 obtained from the *I–V* characteristics are given. The rectification ratio is the same, ideality factor less for the sample MQW1 but series resistance larger than for the MQW 2. This may be due to the wider barriers in the QWs for this sample (cf. Fig. 4a and b).

The *I–V* curves and Arrhenius plots of saturation current for the samples MQW1 and MQW2 are shown in Fig. 8. and in Fig. 9, respectively.

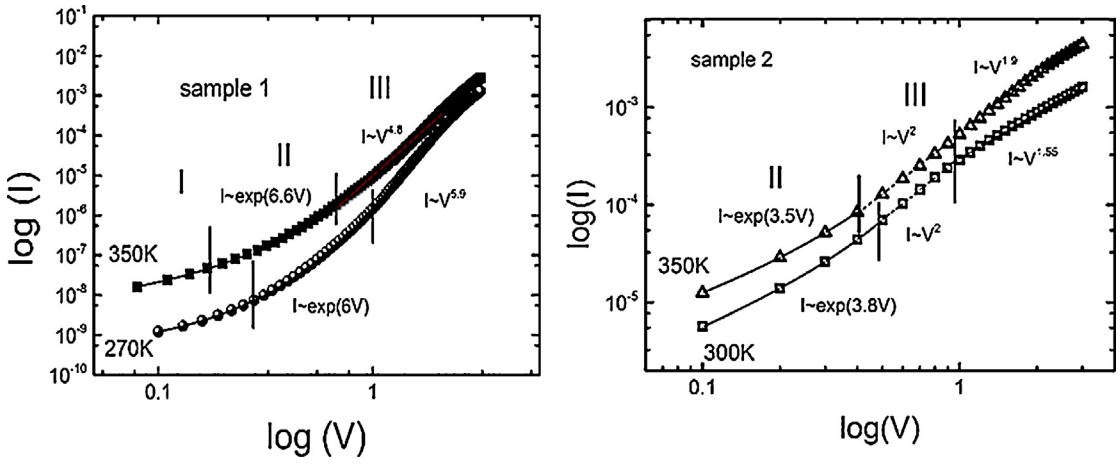

Fig. 7. *I–V* curves for the samples 1 and 2 at two different temperatures, shown in a double logarithmic scale. The regions I–III, governed by different mechanisms of current transport are separated by vertical lines.

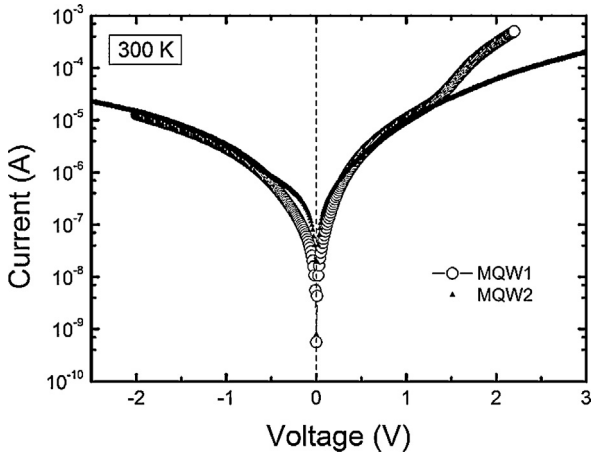

Fig. 8. Room temperature *I–V* characteristics for the samples MQW1 and MQW2.

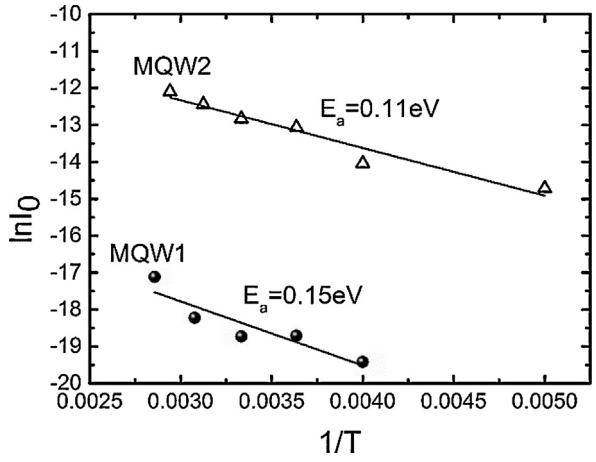

Fig. 9. The Arrhenius plots of the saturation current for the samples MQW1 and MQW2.

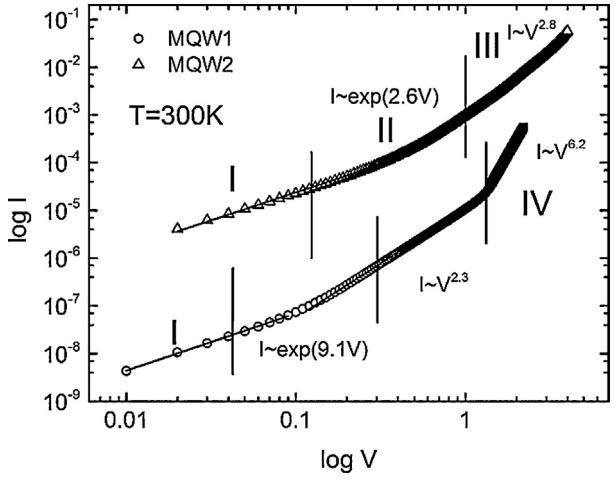

Fig. 10. *I–V* curves for the samples MQW1 and MQW2, shown in a double logarithmic scale.

A linear fit of the plots shown in Fig. 9 yields activation energy of about 0.15 eV and 0.11 eV, for the samples MQW1 and MQW2, respectively. Like in the case of the samples 1 and 2, both values are much smaller than the band gap energy of ZnO.

The log–log plots are presented in Fig. 10 for both MQW1 and MQW2 samples. At a low voltage bias (<0.1 V for the sample MQW1 and 0.04 V for the sample MQW2) labeled as region I, the slope of the plots are close to 1, indicating the Ohmic region, due to the tunneling current. At a larger voltage bias, region II, multitunneling capture emission current dominates. This conclusion is based on the same arguments like in the case of sample 1 and 2. In the region III SCLC dominates. The slope $m > 2$ for both samples indicates the SCLC with contribution of traps. It must be emphasized that the concentration of traps in both samples is large, because neither of the curves reach the voltage trap filled limit, V_{TFL}. In the case of the sample MQW1 region IV can be distinguished with a very high value of m, indicating exponentially distributed traps.

It may be concluded, that the transport mechanism in the samples MQW1 and MQW2 is dominated by multitunneling capture-emission current at lower voltages (region I), and at higher voltages (region II) it is dominated by space-charge-limited current.

Now we should comment on the activation energy obtained from the Arrhenius plots of saturation currents for all of the studied samples. The value of activation energy is between 0.1 and 0.25 eV, depending on an HJ. The activation energy reported in Ref. [5] was about 0.18 eV for ZnO layers grown on Si by photoinduced electro deposition method and 0.26 eV for nc-ZnO/p-Si by the sol–gel technique [4], thus our results are close to those obtained by others. The question is which of the terms in Eq. (4) dominates. If the first one than the activation energy is related to electron capture at trap levels. The electron traps in ZnO of activation energy about 0.1 eV were reported by several authors. In Ref. [21] a defect level with E_a = 0.065 eV was found for ZnO layers grown in Zn-rich conditions by means of MBE method. Roth and Williams have reported a few shallow donor levels in ZnO formed by oxidation method with activation energies within the range of 0.03–0.06 eV [22]. In [23] a shallow donor level of 60–70 meV is claimed to be typical for bulk ZnO grown by vapor-phase method. Moreover, it is also suggested that Al_{Zn} is responsible for such a donor level since Al is a common contaminant in ZnO. Hydrogen is also very often considered as a cause of shallow donor levels since it is present in many techniques commonly used for ZnO growth, even in high vacuum systems such as MBE [24,25].

If the second term in Eq. (4) is more significant, the hole emission prevails and the activation energy would be a greater distance from the Fermi level to the valence band. Based on the assumed band diagram, shown in Fig. 2b, this term cannot be dominant because the distance from the top of the valence band to the Fermi level is much larger than the activation energy of 0.1–0.25 eV.

5. Conclusions

It was found that the multitunneling capture-emission current dominates the low forward bias current transport in the studied n-ZnO or $Zn_{0.9}Mg_{0.1}O$/p-Si heterojunctions. It may be assumed that the electron trap of activation energy 0.1–0.25 eV is responsible for the MTCE mechanism in these HJs. At a larger voltage bias space charge limited current accompanied by traps prevails. Both current transport mechanisms indicate that there is a large concentration of defects at the interface of the HJs. This conclusion has been already confirmed by deep level transient spectroscopy studies run by us for the sample 1 [9]. Obtained results are in accordance with the data reported by other authors for n-ZnO/p-Si HJs grown by various technologies [6–8].

As far as the HJs n-ZnO/p-Si are compared to the n-$Zn_{0.9}Mg_{0.1}O$/p-Si HJs it must be pointed out that the rectifying properties are better for the latter ones. This may be due to the fact, that the ZnO/Si HJ forms types II HJ [12] while the latter one type I. Moreover, the presence of a thin MgO layer at the $Zn_{0.9}Mg_{0.1}O$/Si interface improves the rectifying properties of the diodes. It has to be emphasized that the analysis of current transport mecha-

nisms in the n-$Zn_{0.9}Mg_{0.1}O$/p-Si HJs has been done for the first time.

Acknowledgements

This work has been partially supported by the statutory grant Wroclaw University of Science and Technology, S50013, by the project of National Laboratory of Quantum Technologies (POIG. 02.02.00-00-003/08-00) and NCN project DEC-2013/11/B/ST7/01385. One author (M.A.P.) would like to acknowledge the support by the NCN project DEC-2013/09/D/ST5/03881.

References

[1] J.D. Ye, S.L. Gu, S.M. Zhu, W. Liu, S.M. Liu, R. Zhang, Y. Shi, Y.D. Zheng, Electroluminescent and transport mechanisms of n-ZnO/p-Si heterojunctions, Appl. Phys. Lett. 88 (2006) 182112(1)–182112(3).
[2] S. Aksoy, Y. Caglar, Effect of ambient temperature on electrical properties of nanostructure n-ZnO/p-Si heterojunction diode, Superlattices Microstruct. 51 (2012) 613–625.
[3] H.L. Lu, Y.Z. Gu, Y. Zhang, X.Y. Liu, P.F. Wang, Q.Q. Sun, S.J. Ding, D.W. Zhang, Effects of ZnO seed layer annealing temperature on the properties of n-ZnO NWs/Al_2O_3/p-Si heterojunction, Opt. Express 22 (2014) 22184–22189.
[4] Y. Zhang, J. Xu, B. Lin, Z. Fu, S. Zhong, C. Liu, Z. Zhang, Fabrication and electrical characterization of nanocrystalline ZnO/Si heterojunctions, Appl. Surf. Sci. 252 (2006) 3449–3453.
[5] J.D. Lee, C.Y. Park, H.S. Kim, J.J. Lee, Y.G. Choo, A study of conduction of ZnO film/p-Si heterojunction fabricated by photoinduced electrodeposition under illumination, J. Phys. D: Appl. Phys. 43 (2010) 365403–365408.
[6] S.Y. Liu, T. Chen, Y.L. Jiang, G.P. Ru, X.P. Qu, The effect of postannealing on the electrical properties of well-aligned n-ZnO nanorods/p-Si heterojunction, J. Appl. Phys. 105 (2009) 114504(1)–114504(5).
[7] S.R. Tankio Djiokap, Z.N. Urgessa, C.M. Mbulanga, A. Venter, J.R. Botha, Transport characteristics of n-ZnO/p-Si heterojunction as determined from temperature dependent current–voltage measurements, Physica B 480 (2016) 68–71.
[8] C. Klingshirn, ZnO: from basics towards applications, Phys. Status Solidi B 244 (2007) 3027–3073.
[9] E. Placzek-Popko, K.M. Paradowska, M.A. Pietrzyk, Z. Gumienny, P. Bieganski, A. Kozanecki, Deep traps and photo-electric properties of p-Si/MgO/n-$Zn_{1-x}Mg_xO$ heterojunction, J. Appl. Phys. 118 (2015) 074501–074507.
[10] S.M. Sze, K.K. Ng, Physics of Semiconductor Devices, John Wiley& Sons, New Jersey, 2007.
[11] S. Adachi, Handbook on Physical Properties of Semiconductors II–VI Compound Semiconductors, vol. 3, Springer, Berlin, 2004.
[12] K.E. Knutsen, R. Schifano, E.S. Marstein, B.G. Svensson, A.Yu. Kuznetsov, Prediction of high efficiency ZnMgO/Si solar cells suppressing carrier recombination by conduction band engineering, Phys. Status Solidi A 210 (2013) 585–588.
[13] A.R. Riben, D.L. Feucht, *n*Ge/*p*GaAs heterojunctions, Solid-State Electron 9 (1966) 1055.
[14] H. Matsuura, T. Okuno, H. Okushi, K. Tanaka, Electrical properties of n-amorphous/p-crystalline silicon heterojunctions, J. Appl. Phys. 55 (1984) 1012–1019.
[15] P. Rosales-Quintero, A. Torres-Jacome, F.J. De la Hidalga-Wade, C. Zúñiga-Islas, W. Calleja-Arriaga, C. Reyes-Betanzo, Superficies Vacío 21 (June (2)) (2008) 1–8.
[16] A. Lampert, P. Mark, Current Injection in Solids, Academic, New York, 1970.
[17] A. Rose, Space-charge-limited currents in solids, Phys. Rev. 97 (1955) 1538–1544.
[18] F. Chaabouni, M. Abaab, B. Rezig, Characterization of n-ZnO/p-Si films grown by magnetron sputtering, Superlattices Microstruct. 39 (2006) 171–178.
[19] F.Z. Bedia, A. Bedia, B. Benyoucef, S. Hamzaou, Electrical characterization of n-ZnO/p-Si heterojunction prepared by spray pyrolysis technique, Phys. Procedia 55 (2014) 61–67.
[20] A.A.M. Farag, W.A. Farooq, F. Yakuphanoglu, Characterization and performance of Schottky diode based on wide band gap semiconductor ZnO using a low-cost and simplified sol–gel spin coating technique, Microelectron. Eng. 88 (2011) 2894–2899.
[21] D.C. Oh, T. Suzuki, J.J. Kim, H. Makino, T. Hanada, M.W. Cho, T. Yao, Electron-trap centers in ZnO layers grown by molecular-beam epitaxy, Appl. Phys. Lett. 86 (2005) 032909-1–032909-3.
[22] A.P. Roth, D.F. Williams, Properties of zinc oxide films prepared by the oxidation of diethyl zinc, J. Appl. Phys. 52 (1981) 6685.
[23] D.C. Look, D.C. Reynolds, J.R. Sizelove, R.L. Jones, C.W. Litton, G. Cantwell, W.C. Harsch, Electrical properties of bulk ZnO, Solid State Commun. 105 (1998) 399–401.
[24] C.G. Van de Walle, Hydrogen as a cause of doping in zinc oxide, Phys. Rev. Lett. 85 (2000) 1012–1015.
[25] D.M. Hofmann, A. Hofstaetter, F. Leiter, H. Zhou, F. Henecker, B.K. Meyer, S.B. Orlinskii, J. Schmidt, P.G. Baranov, Hydrogen: a relevant shallow donor in zinc oxide, Phys. Rev. Lett. 88 (2002) 045504-1–045504-4.